# Lab on a Chip

Accepted Manuscript






ROYAL SOCIETY OF CHEMISTRY

www.rsc.org/loc

## Graphical abstract

An environment-friendly and flexible paper based energy harvesting with simple configuration is proposed using a principle of reverse electrodialysis (RED). RED is a clean and sustainable blue energy, which converts Gibbs free energy into electricity by salinity gradients, but its performance has been limited by a pump power for delivering electrolytes. Owing to the intrinsic capillary flow in paper, this pump loss could be successfully saved, which corresponds to 25.8% of the generated maximum power. By thoughtful analysis about voltage-current experiment and capillary flow rate in paper channel, the ideal channel design interfacing with the selective membrane was determined and the maxim power and power density was achieved as 55 nW and 275 nW/m$^2$. Since all materials and fabrication process are cost effective and simple, the proposed device can be expected as a clean, sustainable, and easily operable power source for disposable diagnostic device.

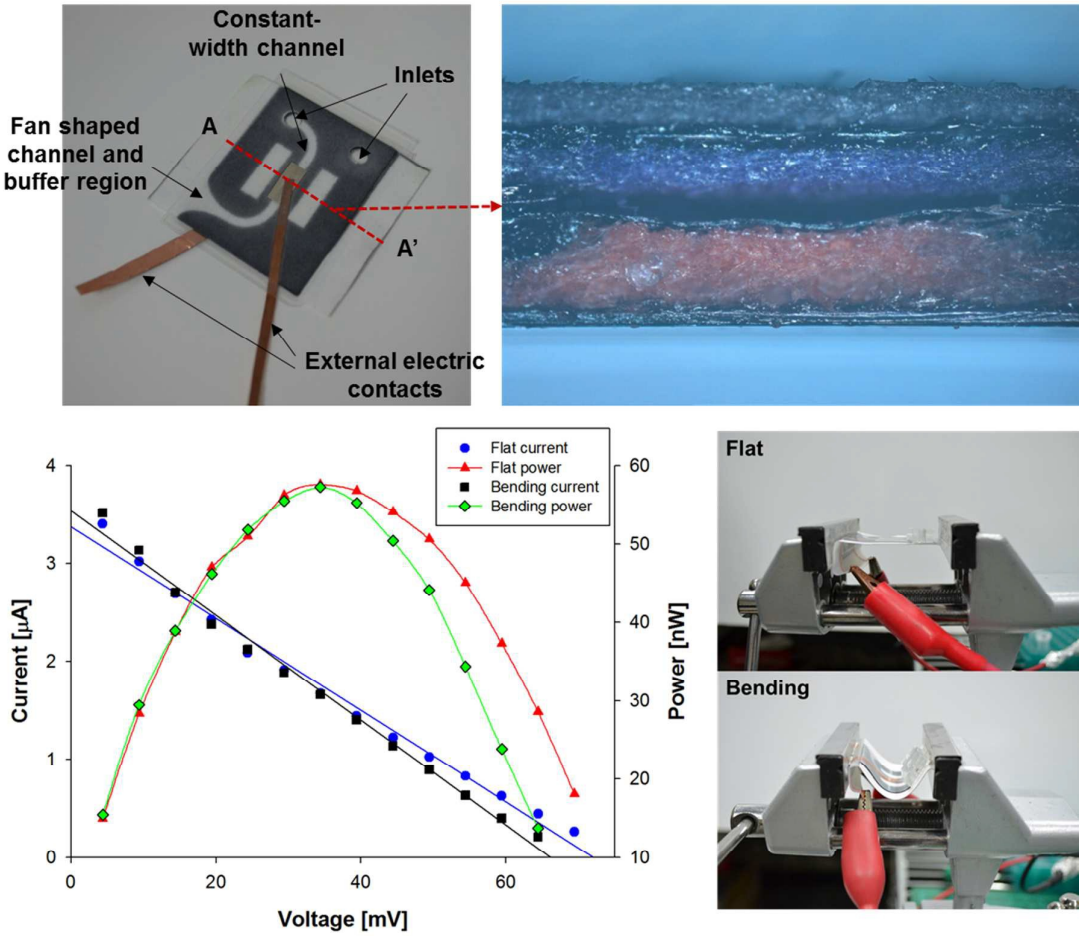

# Paper based Energy Harvesting from Salinity Gradient

Hyung Kwan Chang[1], Eunpyo Choi[1] and Jungyul Park[1,*]

[1]Department of Mechanical Engineering, Sogang University, 35 Baekbeom-ro, Mapo-gu, Seoul, 04107, Korea

[*]Correspondence should be addressed to Prof. Jungyul Park

Tel.: +82 2 705 8642; fax: +82 2 701 7075.

E-mail: sortpark@sogang.ac.kr

**ABSTRACT**

Paper based microfluidic device has many advantage such as low cost, flexibility, light weight and easy disposability. Especially, since intrinsically it can generate capillary-driven flow (no pumps are needed), paper based microfluidic devices are widely used for analytic or diagnostic platform. Along with the advancement in microfluidic paper based analytical devices (μPADs), energy generation using paper materials has received significant attention. In this study, an environment-friendly and flexible paper based energy harvesting with simple configuration is demonstrated by using a principle of reverse electrodialysis (RED). The RED is a promising clean energy generation method, which converts Gibbs free energy into electricity by salinity gradients without discharging any pollutants. However, the power efficiency in the conventional RED device is limited by the essential requirement of an active pumping for providing high and low concentrated electrolytes. The capillary pumping from the proposed paper based RED can save this waste of energy, and moreover, the flexible device is realized with cost effective materials and simple fabrication step, and environmental friendly. By thoughtful analysis about voltage-current experiment and capillary flow rate in paper channel, the optimized channel width interfacing with the selective membrane is determined as 2 mm and the maxim power and power density are achieved as 55 nW and 275 nW/cm$^2$, respectively. 25.8% of the generated maximum power is successfully saved by realizing the pumpless RED system. This paper based RED device can be integrated directly with μPADs as a practical application.

## INTRODUCTION

Since development of the microfluidic devices using polydimethylsiloxane in the 1990s, microfluidics have made great progress in application.[1] Developers of microfluidic devices are often interested in fabricating the devices with the cutting edge technology or novel materials, whereas the end-user are interested in cheap, simple, and user-friendly technologies that solve their own problem. In order to satisfy this demand, paper-based microfluidic devices were proposed, which have been widely used as point-of-care diagnostic system such as healthcare, environmental safety, animal health, and food quality.[2] Along with the advancement in paper based analytical devices (μPADs), recently energy generation using paper materials has received significant attention, because of (1) the preference for the direct integration with μPADs as power sources[3] and (2) and superior property in paper materials for achieving high-power performance.[4, 5]

Until so far, several types of paper based power sources have been reported including fuel cells, lithium-ion batteries, supercapacitors etc.[6] However, most previously developed paper-based power sources configuration requires many functional layers to be deposited onto paper, and complex design and fabrication processes. Moreover, one concern with using electrochemical batteries is usage of non-environmentally friendly material, which is unstable, explosive, flammable, and hazardous electrode or electrolyte.[5]

In this study, in order to address these drawbacks in paper based power generation, an environment-friendly paper based energy harvesting with simple configuration is proposed by using chemical energy conversion from salinity gradient. Revere electrodialysis (RED) based on salinity gradient has received significant attention, because it is clean and sustainable in principle and does not discharge any pollutants or $CO_2$,[7] and can converts Gibbs free energy into electricity with the use of ion selective membrane[8] allowing the selective ion transport as shown in **Figure 1(a)**. RED can be a very suitable power source for μPADs, because it is environmental friendly, and can be realized with very simple configuration with cost-effective way without using the flammable and toxic electrolytes or expensive electrodes like battery and fuel cells. That is, since one of strong merit in μPADs is

disposability, if RED is used as power sources for it, the integrated paper based devices can be easily disposable without considering cost and environmental issues. Moreover, RED can provide electricity sustainably by introducing two concentrated solution, which can be obtained by mixing salt in fresh water.

Various types of RED based power generation had been presented from the large scale system to microfluidic devices.[9-14] Compared to large scale system, microfluidic devices based on nanochannels[12], nanopores[13] or nanochannel networks membrane[14] show more efficient power generation and high power density due to higher ionic flux and a lower fluidic resistance.[10] For examples, Kim *et al*. obtained 0.77 mW $cm^{-2}$ using silica nanochannels,[12] which is one order of magnitude higher than macro-scale RED device. Also, Guo *et al*. estimated power density to be 3-260 mW $cm^{-2}$ with single ion selective track-etched nanopore,[13] which is 2-4 orders of magnitude higher than macro-scale RED device. Therefore, they envision the potential of powering micro/nanodevices without the limitations of batteries or an external power supplies, such as microelectromechanical systems, biomedical implant microdevices, portable personal electronics, and micro/nanorobots.[15, 16] However, to date, even in microfluidic device, an active pump power should be essentially involved in the system to draw two different concentrated solutions into the power generation system and the generated power must be deducted by this energy consumption from the pump also. The proposed paper-based RED devices can remove this inevitable energy consumption from the pump by using intrinsic capillary force in paper, so that more efficient power generation is possible. In addition, the proposed system has simple, disposable, and environmentally friendly structures without using any toxic and flammable electrolytes and can be created with very easy and simple fabrication procedures. The paper based device can generate electricity easily by dropping two concentrated solutions: The asymmetric ion-transport through the cation selective membrane is caused by the concentration gradients and the electrochemical redox reaction on electrodes surface generate electrical power to satisfy electro-neutrality. It has been difficult to create a flexible RED system so far, because the fluidic channels between the swellable ion selective membranes should be separated by spacers and

tightly sealed by hard materials. Since the patterned paper channels and the ion selective membrane are perfectively sealed by lamination, truly flexible and portable RED device can be realized in this study. The power generation performance and the efficiency of energy conversion according to the variation of paper channel geometry and concentration gradients, are carefully investigated from measured current-potential characteristics. Because it is first time to introduce the paper based RED generation, this study can provide the guideline for optimal design for high efficiency. Moreover, it is ready to be integrated with μPADs as a clean, sustainable, and easily operable paper based power source.

## MATERIALS AND METHODS

### Fabrication for paper based RED

In this study, xurography, which is rapid, cleanroom-free, and low-cost prototyping technique, was adopted for simple fabrication of paper based RED.[17] We used whatman filter paper grade 4 for substrate material because it is hydrophilic, homogeneous, flexible, and can induce high flow rate. The filter paper properties of mean porous radius $r_m$~22.5 μm and thickness $t_p$~205 μm are provided by the manufacturers. To control the flow rate in paper-based microfluidic devices, the paper was patterned with hydrophilic and hydrophobic region for imbibition and waterproof, respectively. The wax patterning is appropriate at laboratory scale since it is low-cost and simple method. Example of wax patterning include; (1) wax screening[18], (2) dipping[19, 20] and (3) printing[21-23]. Both wax screening and dipping method, though these does not require high-cost fabrication equipment, they suffer from inflexibility and low reproducibility. In case of wax printing, the entire fabrication process takes just few minute and dimension of the wax printed paper is predictable, so that it is easy to make copies of device. The wax patterned region was designed using design software and printed on whatman filter paper using the solid wax printer (ColorQube 8870, Xerox). The wax printed papers were then placed on a hot plate in order to decompose the wax at 150°C for 120 sec, and the melted wax was spread

through the adjacent area, its nominal spread length was about 300μm.[23] When designing paper channels with narrow width, we should consider this spread effect. Wax patterned papers were designed into two forms, which were for the cover and the fluid channels (referred to hereinafter as the cover paper and the flow channel paper (top and bottom), respectively), as shown in **Figure 1(c)**. The cover paper has two inlets for introduction of the concentrated and diluted solution toward thickness direction, and the two solutions are interconnected into the below flow channel paper. Also, it has a role of preventing evaporation of fluid in the flow channel paper. The flow channel paper consists of an inlet connected directly into the paper channel in the bottom flow channel paper layer and a paper channel contacted with the ion selective membrane. Commercially available Nafion membrane (NR211, Dupont, nominal thickness of $t_m$~25.4 μm) was chosen as the ion selective membrane. To assemble the membrane with the flow channel papers, we cut two double coated tapes (300LSE, 3M, nominal thickness ~71 μm) to have various opening areas (1, 2, 4, 6, 10 mm width and 10 mm length) using a cutting machine (CAMEO, Silhouette Inc.). Ion selective membrane was then sandwiched between the trimmed double coated tapes. The electrodes were made by painting Ag/AgCl ink (011464, ALS Co) to whatman filter paper and then cut into a square shapes. Ag/AgCl electrodes were located at outer sides of the flow channel papers and aligned with opening area in the double coated tapes. Finally, the cover paper, the Ag/AgCl electrode, top and bottom flow channel papers, the ion selective membrane and the double coated tapes were stacked as shown in **Figure 1(b)** and **(c)**. For proper operation, the two different concentrated solutions should be interconnected through ion selective membrane only and except this connection, the two solutions must be perfectively separated. To confirm it, after assembly, the device was laminated using a lamination machine, which could guarantee the sealing between two channels and tight conjunction between the paper channels and ion selective membrane due to a hot pressing.

**Experimental setup for generated power measurement**

**Figure 2(a)** shows a schematic of the experimental system for quantitative measurement of generated

electrical power. The system includes a paper-based RED device, a soucemeter (6487, Keitheley Instrument), and a GPIB board for interface with a computer. The sourcemeter was used as a measurement equipment and an electronic load. We could control the sourcemeter using Labview program (National Instruments) through GPIB interface bus (PCI-GPIB, National Instrument). The sourcemeter recorded the current outputs from the cell while applying various voltage, and the signals was transmitted to the computer.

The electrolyte solution was prepared by diluting potassium chloride (KCl) solution in deionized (DI) water and the pH in the electrolyte solution was measure as 5.6–6.0, similar to that of DI water. The concentration of the diluted solution ($c_L$) was fixed at 0.1 mM while that of the concentrated solution ($c_H$) was changed from 10 mM to 1 M. We obtained each *I-V* curve in a galvanostatic mode. The voltage steps were applied by programmed function and each step was maintained for 100~200 sec in order to acquire steady state *I-V* curves.

**Paper channel design and flow characterization**

The generated power from RED is highly influenced by flow rate. The flow rate in the paper channels depends on channel shape: If the paper channel has constant width (rectangular shape), the flow is governed by Lucas-Washburn equation (the wetted distance $l(t) \propto \sqrt{t}$ ),[24] which means flow rate decreases over time. However, if the paper channel shape is circular or fan, a continuous increase in unwetted pore volumes can lead quasi-stationary flow.[25] For producing steady power generation from RED, the stationary flow rate should be secured, so that as shown in **Figure 1 (c)** and **(d)**, the paper channel was designed as the combination of constant width and fan shape.

Food dyes (Monascus RED 100, ES Ingredients) were used to visualize and characterize flows in the paper-based RED device and these dyes are developed in order to not subject to chromatographic sieving by nitrocellulose. The photograph visualizing the flows in the proposed paper-based is shown in **Figure 3**. The two concentrated flows represented by blue and red food dyes were separately

imbibed through two inlets, and sealed without leakage by the proposed fabrication process.

## RESULTS AND DISCUSSION

**Figure 1(d)** shows the fabricated paper based RED device. Since the devices was laminated, it is very flexible, reliably connected with the measurement system using the external electric contacts and minimizes evaporation from the paper channels. The RED power generation including experimental setup can be represented using the basic circuit element, as shown in **Figure 2(b)**. $E_{app}$, $E_{redox,}$ and $E_{cell}$ are the applied voltage from sourcemeter, the potential by the unequal voltage drop in different electrolyte, and the generated potential in the paper-based RED device, respectively, and simply satisfy the following equation.[12]

$$E_{net} = E_{app} - E_{redox} = E_{cell} - I_{cell} R_{cell} \quad (1)$$

Under asymmetric concentration condition, there exists potential drop between two electrodes and theoretically it is expressed by Nernst relation and given as[26]

$$E_{redox} = \frac{R_g T}{zF} ln \frac{\gamma_{c_H} c_H}{\gamma_{c_L} c_L} \quad (2)$$

Here, $R_g$, $T$, $z$, $F$, $\gamma$ and $c$ are the gas constant, temperature, charge number, Faraday constant, mean activity coefficient, and $c$ is the concentration at the membrane-solution interface respectively, and subscripts $H$ and $L$ represent the high and low concentration solution. According to this theoretical redox potential, we applied voltage steps to measure open circuit voltage ($E_{cell}$). **Figure 4** shows that *I-V* and the generated power curves in normal and the bended device, when the concentration gradients of 1000 folds ($c_L$ = 0.1mM, $c_H$ = 100mM) and $2 \times 10$ mm$^2$ opening area were used. Since the all of materials in our device including papers, Nafion membrane and electrode layers are flexible and

the assemble layers were tightly laminated, the generated power from the bended device is similar with the power from the normal flat device. That is, there is no degradation in power generation by bending the device. *I-V* curves show linear relation in both cases, which means our devices works ohmic region only. Therefore, there is no drastic increase of electrical resistance by ion concentration polarization that happens often at the interface between ion selective membrane and channels. $E_{net}$ was simply calculated with the known value $E_{app}$ and $E_{redox}$ using **Equation (1)**. In this figure, we could obtain $E_{cell}$ from the x-intercept of the graph where the $I_{cell}$ is zero. The diffusion potential generated in the ion selective membrane depends on the ion selectivity in the membrane and it can be expressed as the following equation.

$$E_{cell} = (2t_+ - 1)\frac{R_g T}{zF} ln\frac{\gamma_{c_H} c_H}{\gamma_{c_L} c_L} \quad (3)$$

In this equation, $t_+$ indicates the transference number for the cation, which is an index of cation selectivity. When $t_+ = 1$, it represents a perfect cation selectivity, whereas $t_+ = 0$, it represents a perfect anion selectivity.[27] **Figure 5(a)** shows the variation of transference numbers according to concentration gradient ($c_H$ / $c_L$). The transference numbers tended to decrease as the bulk ion concentration increased due to decrease of electric double layer (EDL). EDL varies from 3 Å to 100 nm for monovalent ions in the 1 to $10^{-5}$ M salt concentration.[28] Here, we used NR-211 Nafion membrane with 3-5 nm range ionic domain size.[29] Especially, EDL is less than 1.0 nm at more than 100mM concentration so that the decrease in transference induces ion selectivity to be reduced. **Figure 5(b)** shows a plot of open circuit voltage according to concentration gradient. The voltage should increase monotonously as the concentration gradient become higher in case of ideal solution and ideal perfect ion-selective membrane ($t_+ = 1$) due to theory of Gibbs free energy. However, in real experiment, the overlapped electrical double layers collapsed rapidly at higher concentration, and it leads the decrease of ion selectivity as expected in **Equation (3)**. Therefore, the open circuit voltage

dropped eventually. The maximum open circuit voltage was obtained under 1000 folds concentration gradient.

**Figure 5(c)** shows the measured current over the different concentration gradient. Under the higher concentration gradient circumstance, ion diffusion was more actively driven and it resulted in higher net diffusion current. However, the ion diffusion current dramatically dropped, where concentration gradient was over 3000-fold. It is because the conductance in nanochannel originate from both contribution between bulk and surface conductance as the following equation.

$$K_N = Fz(c_{K^+}m_{K^+} + c_{Cl^-}m_{Cl^-} + c_{H^+}m_{H^+} + c_{OH^-}m_{OH^-})\frac{wl_m}{t_m} + 2|\sigma|\left[\frac{c_{K^+}}{c_{K^+}+c_{H^+}}m_{K^+} + \frac{c_{H^+}}{c_{K^+}+c_{H^+}}m_{H^+}\right]\frac{w}{t_m} \quad (4)$$

$m_i$ is the mobility of an *i*-type ion and $\sigma$ refers to the volume charge density of the membrane nanopore. As expected the above equation, if the bulk concentration increases, then the first group term grows and overall conductance also rise up. If the bulk concentration increase further, the transference number decrease, which means the second group term drops. Since the first group term gradually increase even in the drop of the second group term, the concentration gradient that induces the maximum current is retarded compared to transference number or open circuit voltage. When the concentration gradient reached at 3000-fold, the current became maximized. Therefore, the maximum power 55 nW ( $P_{max} = \frac{E_{cell}^2}{4R_m}$, $R_m$ is electrical resistance of the membrane) could be achieved at 3000-fold concentration gradient (**Figure 5 (d)**).

RED performance is closely related with the flow rate of the electrolytes and opening area between channels and ion selective membrane. Especially, since the flow rate in paper channel depends on the design of channel, it should be investigated that the effect of paper channel design, which is critical for flow rate and electrical characterization. According to Lucas-Washburn equation, the change of

width in straight channel has no effect on flow rate. However, recently Hong *et al*. demonstrated that the imbibition speed is related on channel width, when the width is narrow.[30] The driving forces via capillarity is notably reduced in the narrow width-paper channel with hydrophobic boundaries, because the surface tension at the boundaries is in an inverse direction to the flow, which retards the imbibition speed. In order to consider the effect for flow rate in RED precisely, constant-width channels (1, 2, 4, 6 and 10 mm) with the same length (36 mm) were patterned and the flow velocity were measured by observing the imbibition of food dyes. **Figure 6** describes comparison of flow speeds from the constant width channels. The average flow speeds with width of 4 ~ 10 mm have similar values (~16.5 μm/sec), but the speeds are decreased in small width channels (~14.0 μm/sec with 2 mm width, ~11.1 μm/sec with 1 mm width). In order to clarify the effect from flow speed in RED performance (conductance, open circuit voltage, efficiency and generated power), we also investigated the electrical characterization with respect to the variation of channel width at 1000-fold gradient condition (**Figure 7**). As shown in **figure 7(a)**, it can be seen that the channel conductance is almost linearly proportional to the width of the channel. The conductance become higher, as the width of channel increases, at the same concentration gradient. The conductance at a width of 2 mm was almost twice that at a width of 1 mm and half that at a width of 4 mm. In case of 6 mm and 10 mm width, the conductance was not increase linearly. From the linear correlation between electrical conductance and channel width, we can infer that the change of electrical resistance from the wax boundary can be ignorable. If the electrical resistance effect from the boundary layer is dominant in paper channel, it should exist nonlinear effect in the small channel, such as the sudden drop of conductance in the small channel. **Figure 7(b)** shows that the open circuit voltage peaked at a width of 2 mm. The diffusion potential should be depend on only the transference number if the concentration gradient is fixed (**Equation (3)**). According to our previous work,[14] the higher interface area may result in the increase in the number of diffused ions including co-ions in the nanopore in the membrane, which can induce hindering the diffusion of counter-ions. As a result, the transference number decreases as the interface area (opening area) between nanochannel or nanoporous membrane

and main channel increases because the number of diffused ions increases: the bulk concentration ratio ($c_H/c_L$) decrease with the higher diffusion in wider ion exchange area. Therefore, it is consistent experimental result that wider paper channel induces lower open circuit potential due to lower transference number. The open circuit voltage at a width of 1mm is slightly smaller than that at a width of 2 mm. Because of the flow speed at a width of 1mm is much slower than that of a 2 mm width channel (**Figure 6**), its RED performance can be degraded due to slow flow speed induced from the effect of hydrophobic wax boundary. We obtained the maximum generated power and power density from our devices as shown in **Figure 7(c)**. Since the generated maximum power is proportional to $E_{cell}^2$, the trends is similar with open circuit voltage. In the smallest channel (1 mm width), the slow flow velocity induces the drop of generated power density and energy conversion efficiency (**figure 7 (d)**). The energy conversion efficiency is defined as the ratio of the output electrical energy to the input energy (Gibbs free energy of mixing) and this efficiency for the maximum power, $\eta$, can be simply expressed by $\eta = (2t_+ - 1)^2 / 2$. The efficiency is lower than the previous studies[12] due to the disturbance of ion transportation by complex internal structures from membranes and shadow effect from paper channels. The maximum power and power density are 55 nW and 275 nW/cm$^2$, respectively, at the width of 2 mm. Recently, there has been an emerging trend of implementing new analytical methods in the paper-based biosensors, such as electrochemical and fluorescence methods,[31, 32] which require an additional source of power for on-chip fluorescence assays, and allow for powering electrochemical detection, as well as other on-chip functions.[32] This source of power should provide sufficient power about microwatt-level power to illuminate a UV LED. We estimate that the proposed will have 55uW and 275 μW/cm$^2$ if the device is developed in 10 parallel with 50 stacks.

As we aforementioned, the net generated power from conventional microfluidic RED device is smaller than the gross power generation because pumping power is required to drive solution through the microchannels. In this reason, the net power output is determined by subtracting the

hydrodynamic loss from the total generated power. The hydrodynamic loss is the product of the pressure drop and the flow rate for two channels of the RED device ( $P_{pump} = 2\Delta pQ$ ).[33] Theoretically, the quasi-steady flow rate in the paper given by $Q \approx k_i W \Delta p / \mu L$ ,[25] where $k_i$, $W$, $L$, $\mu$, and $\Delta p$ are interstitial permeability, width and length of channel, viscosity of solution, and capillary suction pressure, respectively. Therefore, the hydrodynamic loss is proportional to the square of the capillary suction. The driving force for the imbibition is the capillary suction pressure given by $\Delta p = 2\gamma \cos\theta / r_m$ .[34] Here, $r_m$ is a mean porous radius (22.5 μm), $\gamma$ is a surface tension of water (72.8 mN/m), and $\theta$ is a contact angle (82.2°).[25] The capillary suction pressure could be estimated to be 1.65 kPa. To estimate quasi-steady flow rate, we use experimental result of flow rate since interstitial permeability depend on properties of paper, which is determined by experiment. Based on flow speed experimental result using food dyes, the flow rate was calculated as 0.273 μl/min. Therefore, we could estimate the corresponding hydrodynamic power for inducing the equivalent flow rate was ~14.2 nW and it corresponds to 25.8% of the generated maximum power. That is, 25.8% from the generated power can be saved by capillary force in paper channel. When compared to the generated net power density from microfluidic RED using the external hydraulic pump, the power density from the paper based RED is low (refer supplementary information). It is because that the effective opening area interfacing the ion selective membrane is reduced by cellulose networks in paper (shadow effect) and the ion transportation is also hindered, which results in lower ionic current. Also, flow velocity induced by capillary force, is much lower than the flow velocity by hydraulic pump. Therefore, despite of the microfluidic RED device and the proposed device has similar open circuit voltage, the output current of microfluidic RED device higher than that of proposed device. Further investigation should be carried out to address this problem in paper based RED. However, by removing the external hydraulic pump, a truly portable and cost-effective energy harvesting with simple configuration was realized.

Paper based power source has a limited operation time and power because it is developed for single

usages. The Ag-Al galvanic paper-based cell lasted up to 15min[35] and the paper-based battery consisted of copper (Cu), copper chloride (CuCl) in the filter paper and magnesium (Mg) ran for 90min.[3] Therefore, the paper-based energy source based on electrochemical battery limited their application for single-use diagnostic test. However, biofuel cells have long lifetimes more than electrochemical battery. Microbial fuel cells (MFCs) provided the power to light a red LED for more than 30 min[36] and enzymatic biofuel cells (EBFCs) generated stable current density for 12 h continuous operation.[37] In case of the proposed device, its operating time depends on area of fan-shape zone and buffer region, because of the flow in the paper would be zero after solution wets the entire buffer region, resulting in dramatic decrease of power generation. The operating time of the proposed device is wetting time of entire buffer region and it takes over 1 hr (refer **figure S3**). Since disposable biosensors use simple and a few functions requiring small power density only for a couple of minutes, the power sources lasting for over 1 hr are attractive.

## CONCLUSION

For the first time, we proposed an environment-friendly and flexible paper based reverse electrodialysis platform by using simple channel patterning, stacking and lamination, and showed that it can successfully convert the chemical gradient energy into electricity with the advantage of capillary-driven flow. That is, the proposed RED device could save the pump loss which corresponds to 25.8% of the generated maximum power (~14.2 nW) and we confirmed that the power was not degraded by the bending the device. In order to achieve the efficient power generation, the correlation between electrical characteristics (transference number, open circuit voltage, current and power) and paper channel design for flow rate control, was analyzed by quantitative change of concentration gradient ($c_H/c_L$) and area of ion exchange. As a result, the power has the maximum value 55 nW at the width of 2 mm, and its density value is 275 nW/cm$^2$. Since all materials and fabrication process are cost effective and simple, the proposed device can be expected as a clean, sustainable, and easily operable power source for disposable diagnostic device.

**ACKNOWLEDGMENT**

This work was supported by a National Research Foundation of Korea (NRF) grant funded by the Korean government (MSIP) (NRF-2013R1A1A2073271, NRF-2015R1A2A2A04006181).

## REFERENCES


1. G. M. Whitesides, *Nature*, 2006, **442**, 368-373.
2. A. K. Yetisen, M. S. Akram and C. R. Lowe, *Lab on a Chip*, 2013, **13**, 2210-2251.
3. L. Ki Bang, *Journal of Micromechanics and Microengineering*, 2006, **16**, 2312.
4. L. Hu and Y. Cui, *Energy & Environmental Science*, 2012, **5**, 6423-6435.
5. H. Lee and S. Choi, *Nano Energy*, 2015, **15**, 549-557.
6. T. H. Nguyen, A. Fraiwan and S. Choi, *Biosens Bioelectron*, 2014, **54**, 640-649.
7. L. X. Cao, W. Guo, W. Ma, L. Wang, F. Xia, S. T. Wang, Y. G. Wang, L. Jiang and D. B. Zhu, *Energy & Environmental Science*, 2011, **4**, 2259-2266.
8. J. W. Post, J. Veerman, H. V. M. Hamelers, G. J. W. Euverink, S. J. Metz, K. Nymeijer and C. J. N. Buisman, *Journal of Membrane Science*, 2007, **288**, 218-230.
9. J. Kim, S. J. Kim and D.-K. Kim, *Energy*, 2013, **51**, 413-421.
10. L. Cao, W. Guo, W. Ma, L. Wang, F. Xia, S. Wang, Y. Wang, L. Jiang and D. Zhu, *Energy & Environmental Science*, 2011, **4**, 2259-2266.
11. K. Kwon, S. J. Lee, L. N. Li, C. Han and D. Kim, *Int J Energ Res*, 2014, **38**, 530-537.
12. D.-K. Kim, C. Duan, Y.-F. Chen and A. Majumdar, *Microfluid Nanofluid*, 2010, **9**, 1215-1224.
13. W. Guo, L. Cao, J. Xia, F.-Q. Nie, W. Ma, J. Xue, Y. Song, D. Zhu, Y. Wang and L. Jiang, *Advanced Functional Materials*, 2010, **20**, 1339-1344.
14. E. Choi, K. Kwon, D. Kim and J. Park, *Lab on a Chip*, 2015, **15**, 168-178.
15. Z. L. Wang, *Sci Am*, 2008, **298**, 82-+.
16. J. Baxter, Z. X. Bian, G. Chen, D. Danielson, M. S. Dresselhaus, A. G. Fedorov, T. S. Fisher, C. W. Jones, E. Maginn, U. Kortshagen, A. Manthiram, A. Nozik, D. R. Rolison, T. Sands, L. Shi, D. Sholl and Y. Y. Wu, *Energy & Environmental Science*, 2009, **2**, 559-588.
17. X. Yuan, L. Renaud, M. C. Audry and P. Kleimann, *Analytical chemistry*, 2015, **87**, 8695-8701.
18. W. Dungchai, O. Chailapakul and C. S. Henry, *Analyst*, 2011, **136**, 77-82.

19. T. Songjaroen, W. Dungchai, O. Chailapakul, C. S. Henry and W. Laiwattanapaisal, *Lab on a Chip*, 2012, **12**, 3392-3398.

20. Q. He, C. Ma, X. Hu and H. Chen, *Analytical chemistry*, 2013, **85**, 1327-1331.

21. Y. Lu, W. W. Shi, L. Jiang, J. H. Qin and B. C. Lin, *Electrophoresis*, 2009, **30**, 1497-1500.

22. A. W. Martinez, S. T. Phillips, G. M. Whitesides and E. Carrilho, *Analytical chemistry*, 2010, **82**, 3-10.

23. E. Carrilho, A. W. Martinez and G. M. Whitesides, *Analytical chemistry*, 2009, **81**, 7091-7095.

24. E. W. Washburn, *Physical Review*, 1921, **17**, 273-283.

25. S. Mendez, E. M. Fenton, G. R. Gallegos, D. N. Petsev, S. S. Sibbett, H. A. Stone, Y. Zhang and G. P. López, *Langmuir*, 2010, **26**, 1380-1385.

26. N. Lakshminarayanaiah, *Transport phenomena in membranes*, Academic Press, 1969.

27. C. Fry, S. L. E. N and S. Langley, *Ion-Selective Electrodes for Biological Systems*, Taylor & Francis, 2004.

28. J. N. Israelachvili, *Intermolecular and Surface Forces: Revised Third Edition*, Elsevier Science, 2011.

29. J. Peron, A. Mani, X. Zhao, D. Edwards, M. Adachi, T. Soboleva, Z. Shi, Z. Xie, T. Navessin and S. Holdcroft, *Journal of Membrane Science*, 2010, **356**, 44-51.

30. S. Hong and W. Kim, *Microfluid Nanofluid*, 2015, DOI: 10.1007/s10404-015-1611-3, 1-9.

31. H. Liu and R. M. Crooks, *Analytical chemistry*, 2012, **84**, 2528-2532.

32. N. K. Thom, K. Yeung, M. B. Pillion and S. T. Phillips, *Lab on a Chip*, 2012, **12**, 1768-1770.

33. J. Veerman, M. Saakes, S. J. Metz and G. J. Harmsen, *Chemical Engineering Journal*, 2011, **166**, 256-268.

34. A. W. Adamson, *Physical chemistry of surfaces*, Wiley, New York, 3d edn., 1976.

35. N. K. Thom, G. G. Lewis, M. J. DiTucci and S. T. Phillips, *RSC Advances*, 2013, **3**, 6888-6895.

36. A. Fraiwan and C. Seokheun, Balimore, MD, 2013.

37. G. P. M. K. Ciniciato, C. Lau, A. Cochrane, S. S. Sibbett, E. R. Gonzalez and P. Atanassov, *Electrochimica Acta*, 2012, **82**, 208-213.

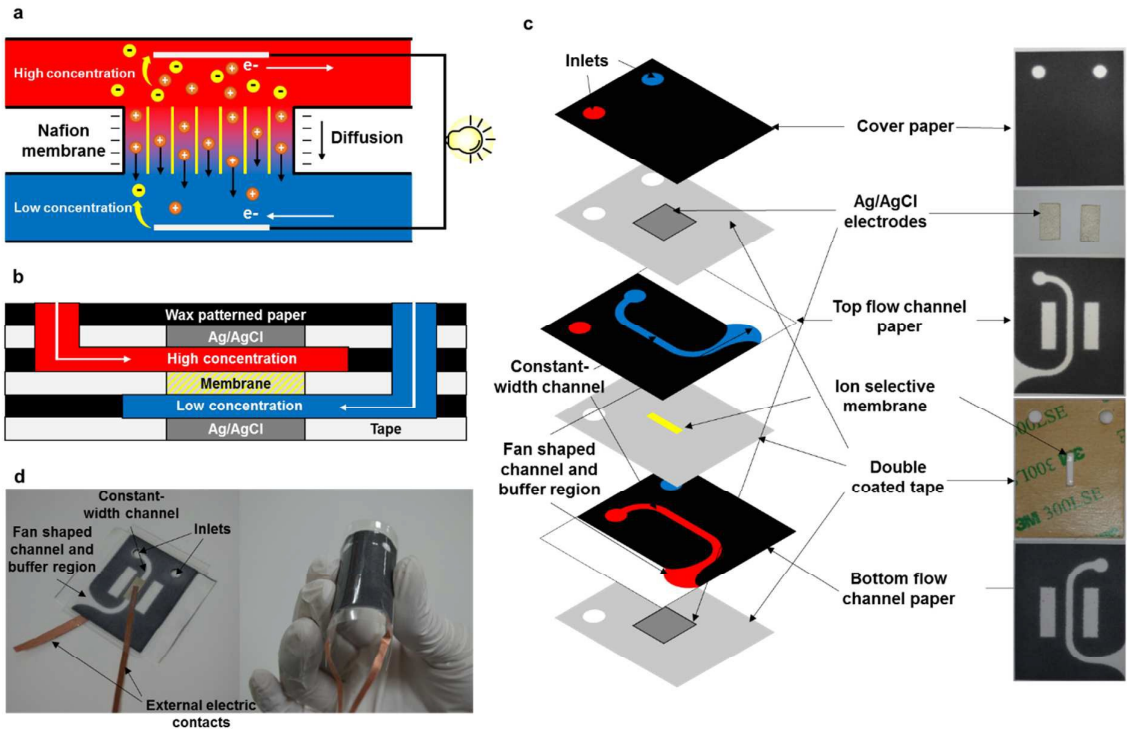


**Figure 1**. (a) Selective cation migration by diffusion through ion selective (Nafion) membrane interconnected with two channels. (b) Schematic illustration of the cross sectional view of the proposed RED devices. (c) Exploded diagram and corresponding photos for each layer in the paper based RED device. (d) Photos of the fabricated paper based RED device.

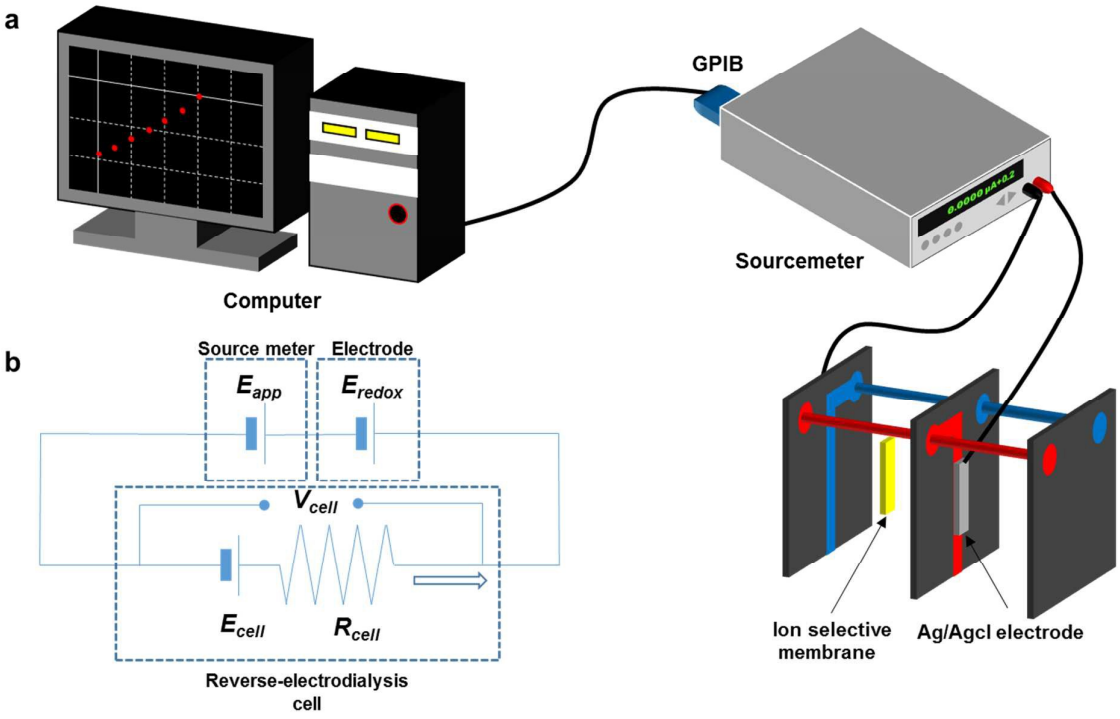


**Figure 2** (a) Schematic of the experimental setup. (b) Equivalent circuits for the paper based RED including experimental setup.

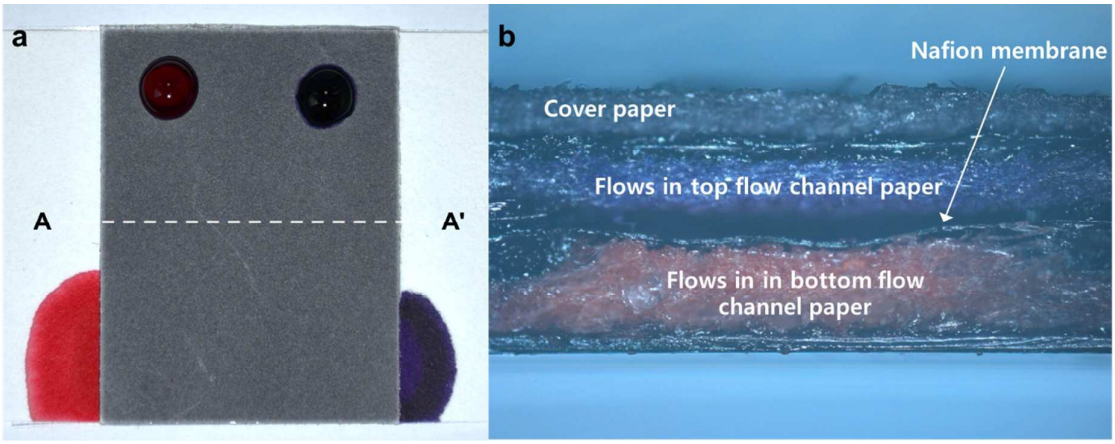


**Figure 3**. (a) Photograph of the paper based RED device with two color dyes imbibition. (b) Microscope image of the cross sectional view in the direction of A-A'. Two dyes are perfectively separated and sealed by the lamination.

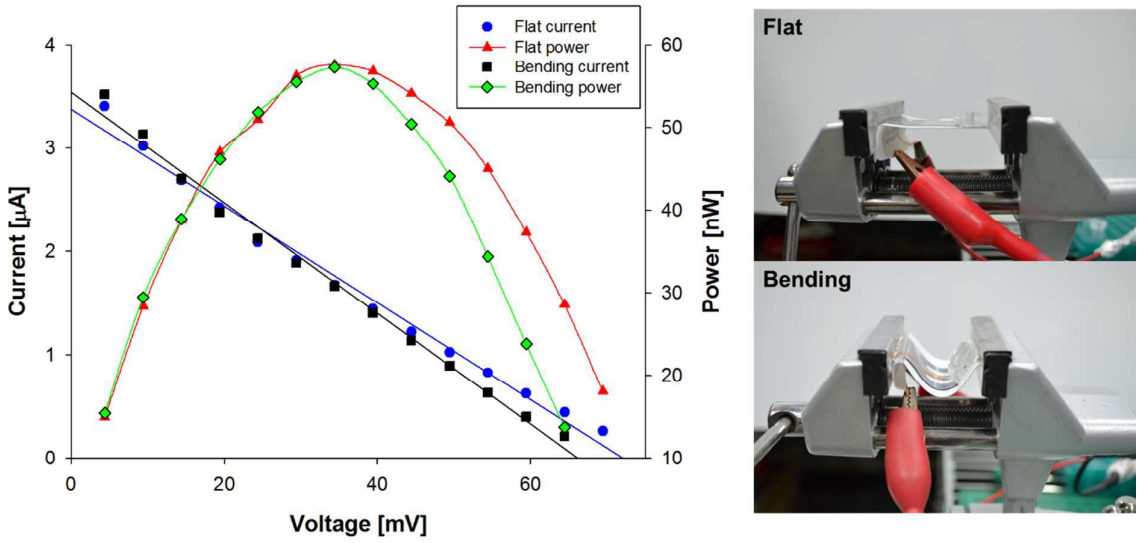


**Figure 4**. Current-potential and power curves from normal (flat) and the bended devices. ($c_H$= 100mM, $c_L$= 0.1mM KCL)

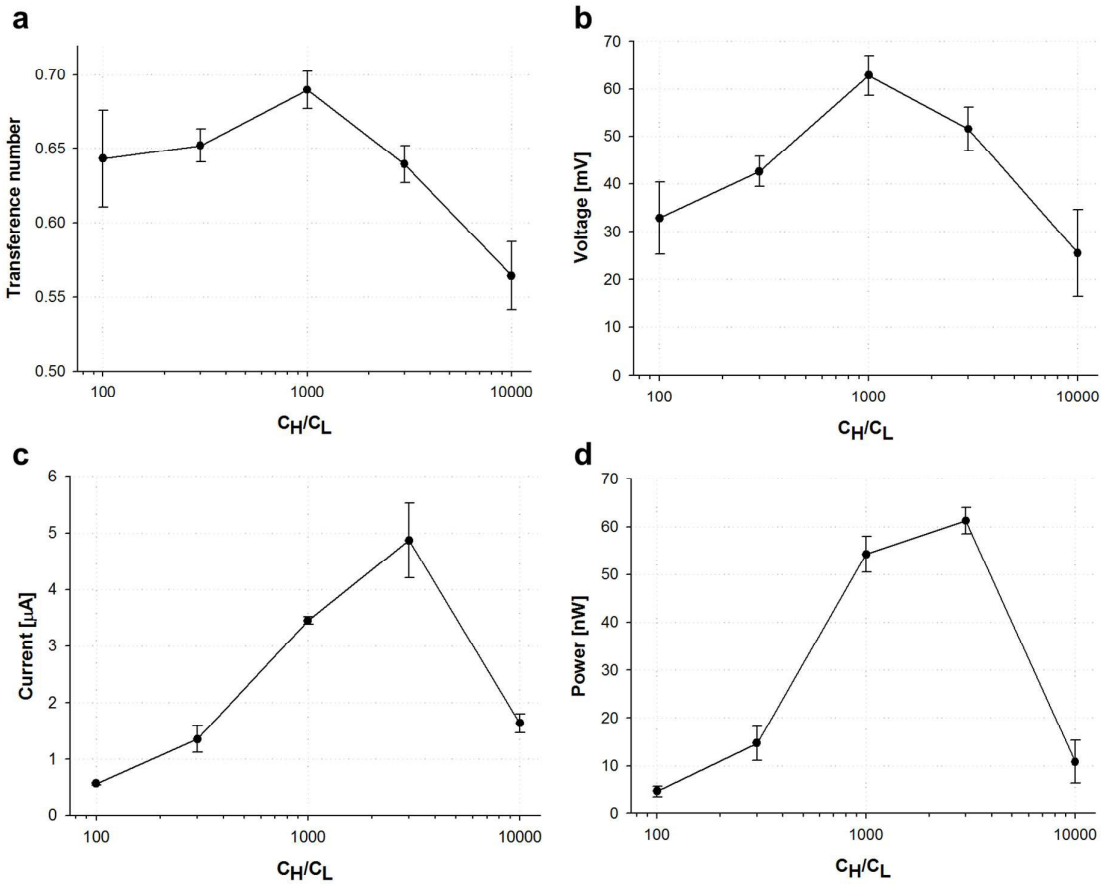


**Figure 5**. Dependence of the (a) transference number, (b) open circuit voltage, (c) current, and (d) maximum power

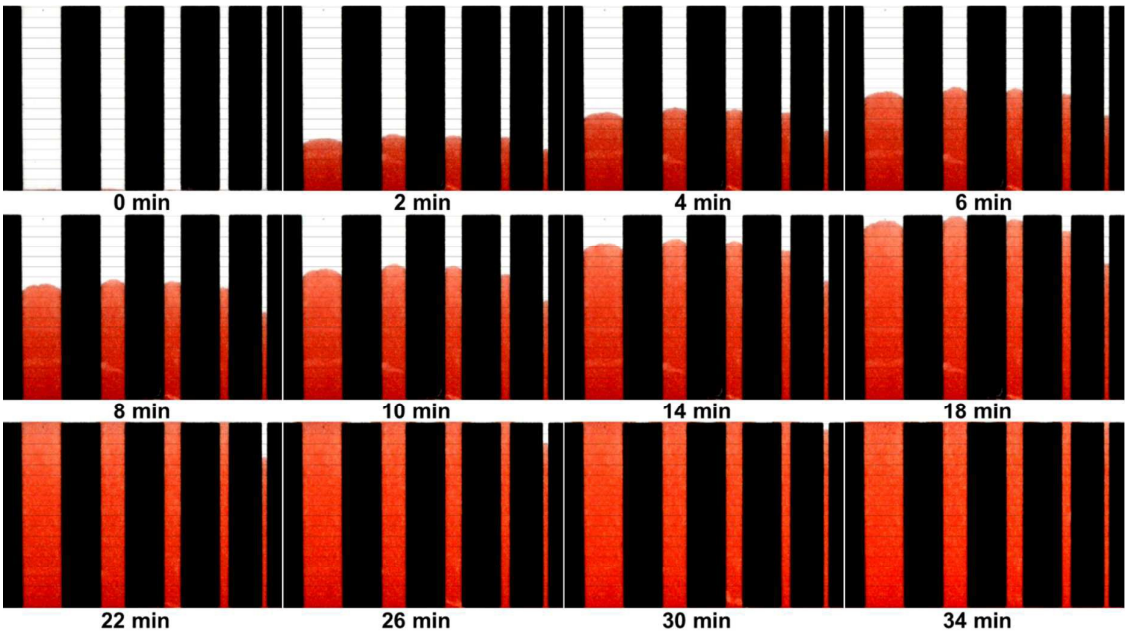


**Figure 6.** Sequential photographies of the dye imbibition experiment. The channel width is 1, 2, 4, 6 and 10 mm from the right of the each picture (interval of horizontal grid = 2 mm). The flow speed decreases over time before the flow reach the end of rectangle shape channel. After then the flow becomes quasi-stationary by the effect of fan shape zone and buffer. The quasi-stationary flow speeds of 4, 6, 10 mm width are similar value (~16.5 μm/sec) but flow speeds are slow for smaller channels: ~14.0 μm/sec with 2 mm width, ~11.1 μm/sec with 1 mm width.

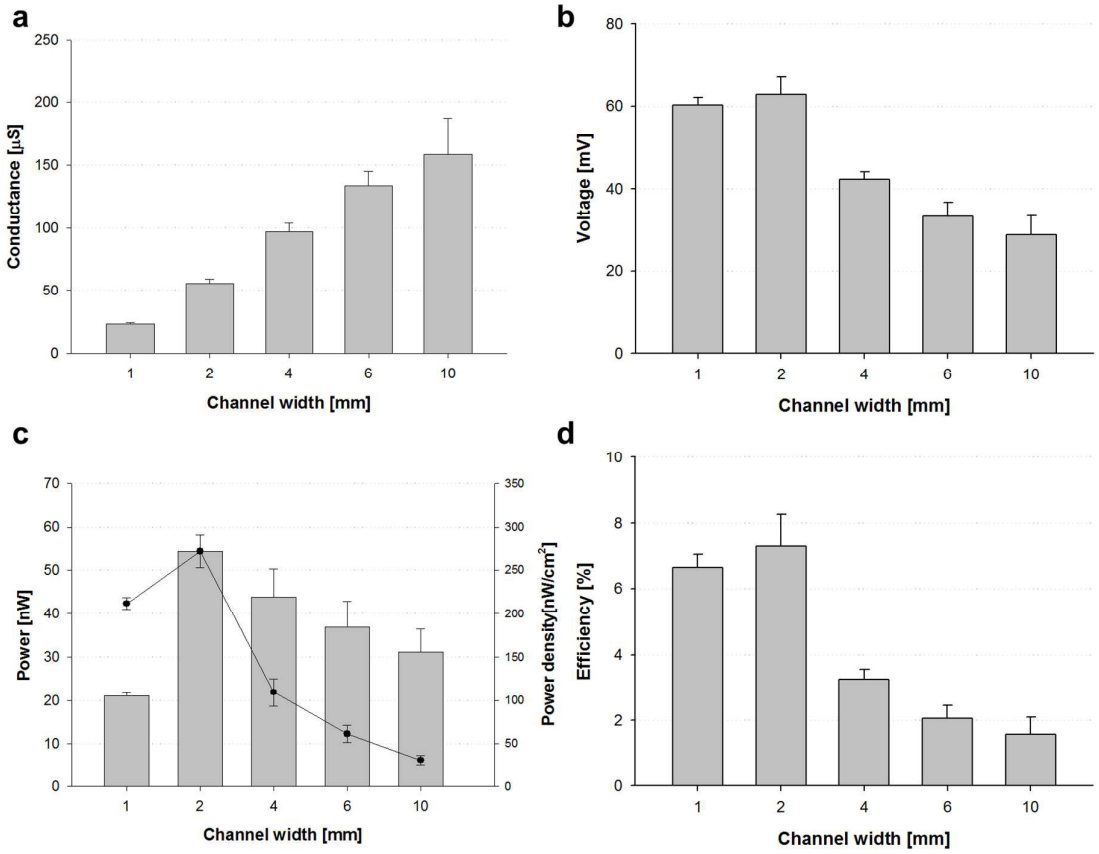


**Figure 7.** Dependence of the (a) conductance (b) open circuit voltage, (c) maximum power (bar graph) and power density (line graph), and (d) energy conversion efficiency on the change of channel width under 0.1mM/100mM KCl concentration gradient